Relationship between Morphological Change and Crystalline Phase Transitions of Polyethylene−Poly(ethylene oxide) Diblock Copolymers. 3. Dependence of Morphological Transition Phenomena on the PE/PEO Segmental Lengths and Its Possible Origins

Weiyu Cao,[†] Kohji Tashiro,*[,†] Hiroyasu Masunaga,[‡] Sono Sasaki,[‡] and Masaki Takata[‡]

Department of Future Industry-Oriented Basic Science and Materials, Toyota Technological Institute, Tempaku, Nagoya 468-8511, Japan, and Japan Synchrotron Radiation Research Institute, Kouto, Sayo, Hyogo 679-5198, Japan

Received: February 17, 2009; Revised Manuscript Received: May 4, 2009

By measurement of the small-angle and wide-angle X-ray scatterings and infrared and Raman spectra and thermal data, microphase separation phenomena have been investigated for a series of polyethylene−poly(ethylene oxide) diblock copolymer (PE-*b*-PEO) in both the heating and cooling processes and compared with the structural changes occurring inside the PE and PEO domains. The complicated morphological changes between lamella, perforated lamella, gyroid, cylinder, and sphere phases were detected for the copolymer with relatively short PE segments. The orthorhombic crystalline structure of PE was kept unchanged in the lamella-to-gyroid transition. When the PE orthorhombic phase transformed to the pseudohexagonal or rotator phase, the gyroid morphology changed to the cylinder. On the other hand, the diblock copolymer with relatively long PE segment was found to show only the lamellar morphology, in which the order−disorder structural transition between the orthorhombic and pseudohexagonal phases occurred in the PE crystal region. As a possibility, the large difference in morphological change between the copolymers with short and long PE segments has been ascribed to the difference in thermal mobility of PE segments, which is controlled by the conformation of chains and their packing mode, i.e., an extended chain or a folded chain. The extended chains may move thermally and actively along the interfacial boundary in addition to the librational motion around the chain axis, resulting in a variety of morphological changes, whereas the thermal motion of the folded chains may be suppressed because of the geometrical constraint and does not cause such a large-scale morphological change from the lamellar structure. This concept, a thermal activity and geometrical constraint, is considered to be quite important in the interpretation of complicated morphological changes observed for many crystalline−amorphous and crystalline−crystalline diblock copolymers when viewed from the molecular level.

Introduction

In a previous paper,[1] on the basis of organized combination of infrared (IR), Raman, wide-angle X-ray diffraction (WAXD), and small-angle X-ray scattering (SAXS) data as well as the thermal data, the phase transitions of polyethylene−poly(ethylene oxide) diblock copolymer (PE-*b*-PEO), E17EO40 and E39EO86, were investigated, where E17EO40 represents the PE and PEO segmental lengths of 17 E (CH_2CH_2) units and 40 EO (CH_2CH_2O) units with the end groups of methyl and hydroxyl groups, respectively. What we revealed for these two diblock copolymers are as follows: (i) They showed the mesoscopic morphological changes between lamella, gyroid, cylinder, and sphere phases in the heating and cooling processes. (ii) During these morphological changes the PE and PEO parts exhibited remarkable structural changes in their individual domains. The PEO crystals melted at around 60 °C, just where the lamellar morphology observed at room temperature transformed to the gyroid morphology. At this moment the PE domains were still in the orthorhombic crystal phase. When the sample was further heated, the PE crystal transformed to the pseudohexagonal phase with more or less disordered conformation, where the gyroid morphplogy changed to the cylinder phase. Once the PE phase melted perfectly at around 100 °C, the whole system transformed to the sphere morphology.

In this way we clarified the relation between the nanoscale morphological change in microphase separation phenomenon and the structure transitions viewed in the molecular level. At this point we need to notice that the morphological change from lamella to gyroid phase (even to cylinder phase) occurs by keeping the crystal lattice of orthorhombic or rotator phase in PE segmental parts, just when the PEO segments are already in the molten state. The system of crystalline PE segments with melted PEO segments is essentially equivalent to the crystalline−amorphous diblock copolymer when viewed from the aggregation states of segments.[3] However, although many studies were searched thoroughly for the phase transition behaviors of general amorphous−crystalline diblock copolymers,[3] we could not find any paper in which the gyroid (and cylinder) structure is created *by keeping the crystalline state of one segmental parts*. A possible origin of this difference might be in such a situation that the chain lengths of PE and PEO segments used in our previous experiment are rather short.[2] The molecular weight of one segment is in the order of several thousands g/mol at most, appreciably lower than that used in many crystalline−amorphous (and crystalline−crystalline[4]) diblock copolymers with the segmental lengths of several tens thousands g/mol. The PE segments of low molecular weight may experience the active thermal motion compared with the

* To whom correspondence should be addressed.
[†] Toyota Technological Institute, Tempaku.
[‡] Japan Synchrotron Radiation Research Institute.

10.1021/jp901442a CCC: $40.75 © 2009 American Chemical Society
Published on Web 06/01/2009

TABLE 1: Molecular Characteristics of PE-*b*-PEO Diblock Copolymers

notation	M_n of PE[a] (g/mol)	M_n of PEO[a] (g/mol)	M_w/M_n
E17EO40	500 (17)	1800 (40)	1.20
E39EO86	1100 (39)	3800 (86)	1.11
E39EO22	1100 (39)	1000 (22)	1.08
E171EO131	4800(171)	5800(131)	1.04

[a] The numbers in parentheses indicate the average number of monomeric units.

segments of high molecular weight. This thermal activity of chain segments in the crystalline state might cause relatively easy change in the aggregation state of chains to induce the transition from lamella to gyroid phase.[5]

It may be predicted that the morphological change and structural phase transitions in the domains may be also affected by the relative chain lengths of the two segments. In the previous paper[1] we used the samples of E17EO40 and E39EO86. Sun et al. used the PE-*b*-PEO copolymer samples of E29EO20.[6] They reported the order−disorder transition in the lamellar morphology. They did not report any transition to gyroid or cylinder. Castillo et al. reported a possibility of the existence of cylinder phase for E82EO18 sample, but the SAXS profile was too broad to find the peaks characteristic of the cylinder phase because of the relatively high amount of side branches in PE segments.[7] The difference in these behaviors might come from the difference in relative segmental lengths of PE and PEO parts. As is well-known, the phase separation strength is governed by the product of a Flory−Huggins χ parameter and an averaged degree of polymerization of individual components N.[3,8] That is to say, the different lengths of PE and PEO chain segments may result in the different transition behavior. However, this concept can be applied to the amorphous−amorphous diblock copolymers.[3] We do not know whether this phase separation strength concept can be applied to the present crystalline−crystalline diblock copolymer case. We have to investigate the effect of relative chain lengths of PE and PEO segments on the above-mentioned transition behaviors in a concrete manner. In other words, it is important to check whether the complicated morphological changes revealed in our previous paper[1] can be observed also for the other kinds of PE-*b*-PEO copolymer, as will be reported in the present paper.

Experimental Section

Samples. PE-*b*-PEO diblock copolymers used in the present experiments are listed in Table 1, which were purchased from Polymer Source Inc. The molecular weight distributions are almost 1.1, relatively sharp for the investigation of phase transitions. According to the catalogue of the company the PE-*b*-PEO diblock copolymer was synthesized by living anionic polymerization reaction with sequence addition of butadiene followed by ethylene oxide and hydrogenation of the butadiene block after recovery of the polymer. The content of 1,2-butadiene segment or the branching of ethyl side groups was negligibly small, as estimated from the NMR data. We measured the infrared spectra of the samples to check the content of ethyl branches of PE, which could be detected from the band at 772 cm^{-1}, characteristic of the ethyl group. No intensity was detected there, supporting the result of NMR.

Measurements. The thermal analysis was performed by measuring the DSC (differential scanning calorimeter) thermograms in the heating and cooling processes using a TA Instruments DSC Q1000 under nitrogen gas atmosphere. The heating and cooling rates were 10 °C/min. The temperature dependence of infrared spectra was measured using a KBr disk prepared by mixing KBr and sample powder homogeneously, where a thermocouple was inserted into a KBr disk to monitor the sample temperature directly. The disk was set into a homemade optical heater cell. The infrared spectra were measured using a Varian FTS7000 Fourier-transform infrared spectrometer by fixing the temperature at constant values stepwise during the measurement. The resolution power was 1 cm^{-1}. The simultaneous measurements of synchrotron SAXS and WAXD data were performed at beamline BL40B2 in SPring-8, Japan, using an incident synchrotron X-ray beam of 1.00 Å wavelength. The sample was sealed off in a glass capillary and set into a Metlar Toledo FP90 DSC heating cell as reported in the previous paper.[1] The WAXD data (Debye−Scherrer rings) were detected using a two-dimensional flat panel (Hamamatsu Photonics, Co. Ltd., Japan) at a sample-to-camera distance of ~8 cm, while the SAXS data were collected at a sample-to-camera distance of ~240 cm through a vacuum pass, behind which an image-intensifier CCD camera (Hamamatsu Photonics) was set. The sample was heated and cooled at a constant rate of 10 °C/min in the temperature region of −40 to 110 °C, during which the WAXD and SAXS data were collected at a time interval of 2 s. The observed two-dimensional data were transferred to the one-dimensional scattering profiles by circularly integrating the rings as function of scattering angle 2θ. The scattering vector q was used for the analysis of these profiles, where $q = (4\pi/\lambda)\sin(\theta)$ with an X-ray wavelength λ. The scattering angles were corrected on the basis of the scattering angles data measured for standard samples (silicon for WAXD and hen tendon collagen for SAXS). The size of incident X-ray beam was about 500 × 300 μm^2, and no correction for slit function was made in the data analysis. The intensity fluctuation of incident X-ray beam was negligibly small because of the so-called TOP-UP operation of synchrotron intensity.

Results and Discussion

In the following several sections we will describe the phase transition behaviors detected for a series of PE-*b*-PEO diblock copolymers listed in Table 1. In the previous paper[1] we reported the data for E17EO40 and E39EO86 samples mainly in the heating process. But the cooling data are also important to check the reversibility of the transitions. Therefore, we will include the data of E17EO40 and E39EO86 samples also for comparison with the other samples.

(1) E39EO22. Figures 1 and 2 show the temperature dependences of SAXS profile measured for E39EO22 sample in the q ranges of 0.3−0.6 and 0.6−1.9 nm^{-1}, respectively. At ambient temperature, the SAXS profile was that typical of lamellar morphology. A series of broad peaks were detected at the position ratios of $q/q_1 = 1:2:3...$ ($q_1 = 0.43$ nm^{-1}). At around 60 °C the peaks became sharper and several peaks were newly detected in the higher q range, which were assigned to the peaks of gyroid phase: $q/q_1 = 1:1.83:3.00...$[8] Between the lamella and gyroid phases the SAXS peaks showed different behavior. For example, the main peak at 0.47 nm^{-1} and the third peak at 1.57 nm^{-1} shifted to higher q direction with an increase of temperature, while the peak at around 0.95 nm^{-1} shifted to the lower q side and became very weak. The peaks at 0.47 and 1.57 nm^{-1} transferred apparently continuously to the peaks of gyroid phase and may be assigned to the perforated lamellar phase appearing between the lamellar and gyroid phases. The peak at 0.95 nm^{-1} may be of the lamellar phase. At 70 °C the gyroid peak at 0.52

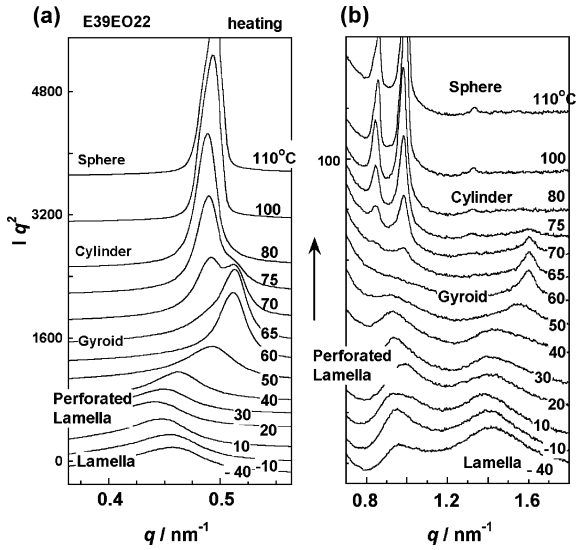

Figure 1. Temperature dependence of SAXS profiles measured for E39EO22 diblock copolymer in the heating process in the q ranges of (a) 0.35−0.75 nm^{-1} and (b) 0.7−1.8 nm^{-1}.

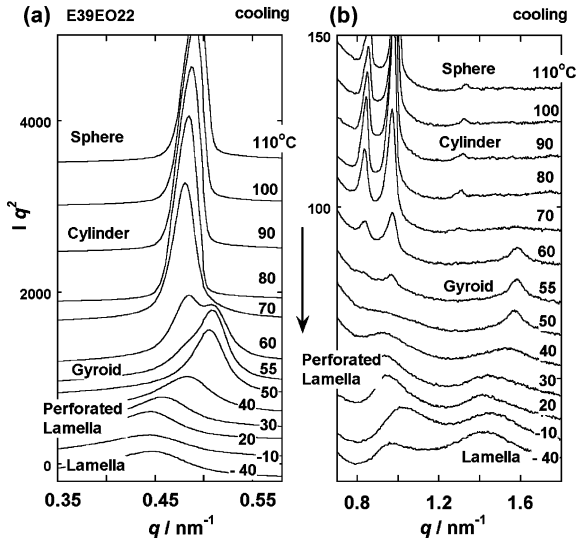

Figure 2. Temperature dependence of SAXS profiles measured for E39EO22 diblock copolymer in the cooling process in the q ranges of (a) 0.35−0.60 nm^{-1} and (b) 0.7−1.7 nm^{-1}.

nm^{-1} became lower and a new peak was detected at $q = 0.48$ nm^{-1}. The peaks in the higher q range also increased in intensity and were assigned to the cylinder phase ($q/q_1 = 1:1.73:2:2.65...$, $q_1 = 0.48$ nm^{-1}). It is noted here that the SAXS peaks of gyroid and cylinder phases were coexistent in the transition range of 65−75 °C, indicating the transition of the thermodynamic first-order type. The scattering profile at 110 °C seems to be an overlap of cylinder and sphere morphologies, although the sphere peaks were few. In Figure 3 are shown the temperature dependences of SAXS intensities estimated for these phases in the heating and cooling processes. The transition occurred almost reversibly among the following phases:

lamella−perforated lamella−gyroid−cylinder−sphere

Figure 4 shows the temperature dependence of WAXD profiles measured in the heating and cooling processes of this sample. In the cooling process from the melt, for example, the PE peak assigned to the orthorhombic 110 reflection started to

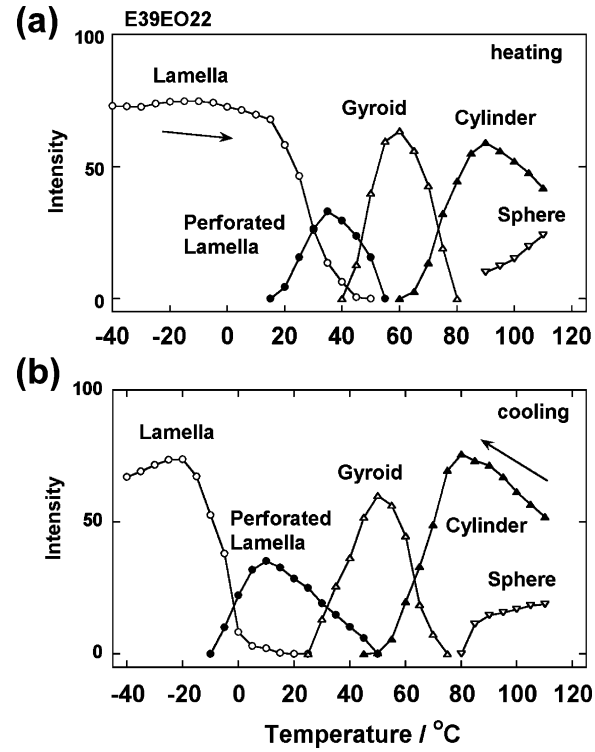

Figure 3. Temperature dependence of SAXS intensity of the peaks characteristic of each morphology in the (a) heating and (b) cooling processes of E39EO22 copolymer.

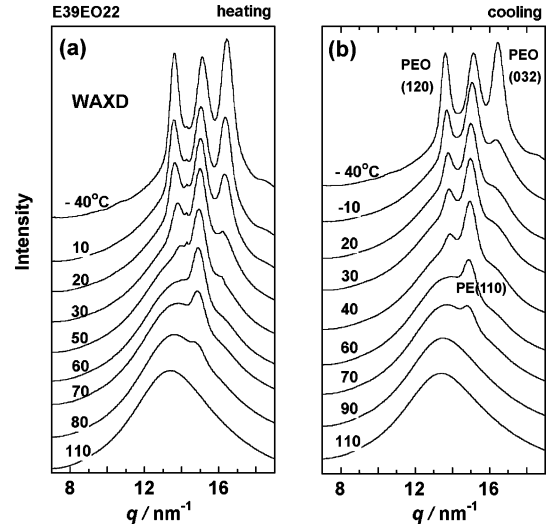

Figure 4. Temperature dependence of WAXD profiles measured for E39EO22 diblock copolymer in the (a) heating and (b) cooling processes.

appear at around 80 °C, increased in intensity steeply, and saturated in the low temperature region as shown in Figure 5. (The peak of the pseudohexagonal phase of PE might be observed at first but was difficult because of the overlap of a strong halo peak.) The X-ray peaks of PEO were observed to behave at the two stages.[9] In the temperature region from 50 to −10 °C, the 120 reflection increased in intensity and the 032 reflection was much weaker. At around −10 °C the 032 reflection started to increase remarkably and exceeded the intensity of the 120 reflection. Similar behavior was observed also in the infrared spectra as shown in Figure 6. In the cooling process, the infrared spectral profile of PEO became relatively sharp below 50 °C and was sharpened more remarkably below

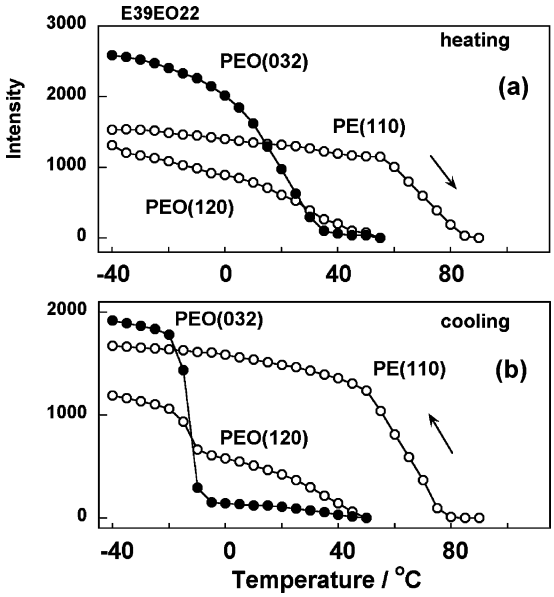

Figure 5. Temperature dependence of WAXD intensities of the PEO 120 and 032 reflections and PE 110 reflection estimated in the (a) heating and (b) cooling processes of E39EO22 copolymer.

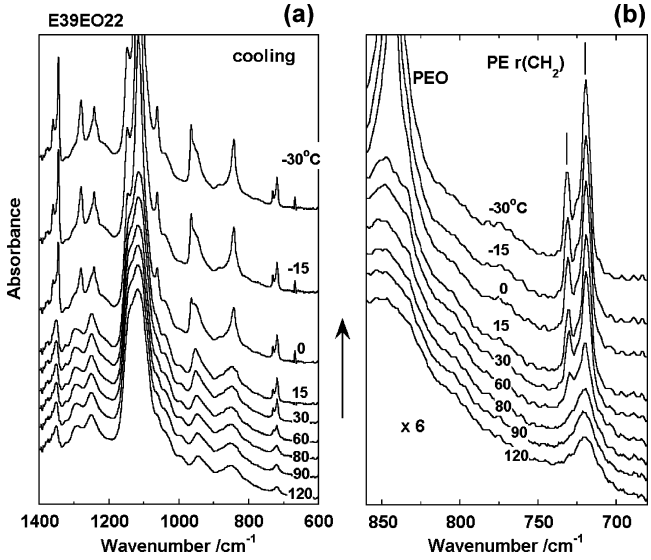

Figure 6. Temperature dependence of infrared spectra measured for E39EO22 diblock copolymer in the cooling process: (a) 1400−600 cm^{-1} and (b) 860−680 cm^{-1}.

0 °C. In the crystalline phase of the high temperature region the conformation of PEO chains was more or less disordered judging from the relatively broad spectral profile while it became more regular in the low temperature region. These observations are consistent with the above-mentioned WAXD data. The IR peaks intrinsic to the PE segments showed the changes between the orthorhombic, pseudohexagonal (rotator), and molten phases, as already detected for E17EO40 and E39EO86 samples.[1] Immediately below the melting point, the infrared band of the rotator phase was observed at around 721 cm^{-1}.[10] In the cooling process this band changed to a pair of bands at 720 and 730 cm^{-1}, characteristic of the orthorhombic phase. The relative intensity of 730 cm^{-1} band was appreciably lower compared with the case of structurally regular orthorhombic unit cell as seen well for pure *n*-alkane crystal.[11] This indicates an existence of a packing disorder of PE chain segmental parts even at such a low temperature as −30 °C.

Figure 7 shows the temperature dependences of all the experimental data collected for E39EO22 diblock copolymer in comparison with the DSC thermograms. For example, in the case of the cooling process from the melt, the sphere phase exists in the high temperature region, in which the molecular chains are in the amorphous state as known from the WAXD halo peak and the broad infrared band profile. In the cylinder phase region (90−70 °C) the rotator phase of PE segments starts to appear as detected in the IR (and WAXD) data. By cooling further, the gyroid phase increases in intensity. At almost the same time the orthorhombic crystalline phase starts to appear in the PE segmental side. At a lower temperature the lamellar morphology is observed via perforated lamella and both of PE and PEO segments exist as the crystalline phases. The PEO chains are more highly regularized below −10 °C. In Figure 7 it noted that the DSC thermograms were appreciably broad compared with the normal thermograms detected for pure *n*-alkane and PEO. The thermograms are broad because they are considered to reflect the enthalpy changes originating from the crystalline phase transitions in the domains of each component and those of morphological changes of the whole sample.

In this way the orthorhombic crystal lattice of PE segments exists in the domains of the lamellar and gyroid morphological phases. The rotator phase of PE segments exists in the cylinder phase. We know the very intimate relation between the mesoscopic morphological changes and the structural changes in the domains of each segments. If the orthorhombic lattice of PE is thermally static and rigid, such a large change in morphology from cylinder to gyroid and lamella is difficult to occur. These morphological changes can be understood reasonably if the PE chain segments of relatively short length become thermally active even in the orthorhombic crystal lattice. We know such an example that pentadecanoic acid shows the orthorhombic-to-orthorhombic packing mode change in a relatively narrow temperature region around 46 °C, in which the zigzag chain segments experience the flip-flop motion to change their orientation direction in the *ab* plane.[12] In this transition the splitting of infrared bands intrinsic to the orthorhombic packing mode is observed, but the molecular chains experience remarkable cooperative rotational motion around the chain axis. A similar situation might be in the present case of E39EO22. A detailed discussion will in a later section.

(2) E17E40 and E39EO86. The phase transition behaviors of these two kinds of diblock copolymers were already reported in our previous paper.[1] Therefore, only the temperature dependences of the various experimental data are given here in both the heating and cooling processes as shown in Figures 8 and 9, respectively. In these cases, the transition occurs reversibly between lamella, perforated lamella, gyroid, cylinder, and sphere phases. (The existence of perforated lamellar phase was added to the previously reported data, since the SAXS data were interpreted more reasonably by assuming the existence of this phase in the transition process from lamella to gyroid phases.)

(3) E171EO131. The DSC thermograms of this diblock copolymer are relatively sharper than the other cases. As shown in Figure 10, clear melting and crystallization peaks were detected in the heating and cooling processes, respectively, in addition to some weak and broad peak at around 60 and 90 °C (cooling). The temperature dependence of SAXS profile measured in the heating process is shown in Figure 11. The SAXS profile at low temperature was broad. All the peaks can be indexed as $q/q_1 = 1{:}2{:}3$ with $q_1 = 0.182$ nm^{-1}. By heating, the peaks became sharper and the peaks were detected at the same ratio: $q/q_1 = 1{:}2{:}3$ with $q_1 = 0.210$ nm^{-1} at 110 °C.

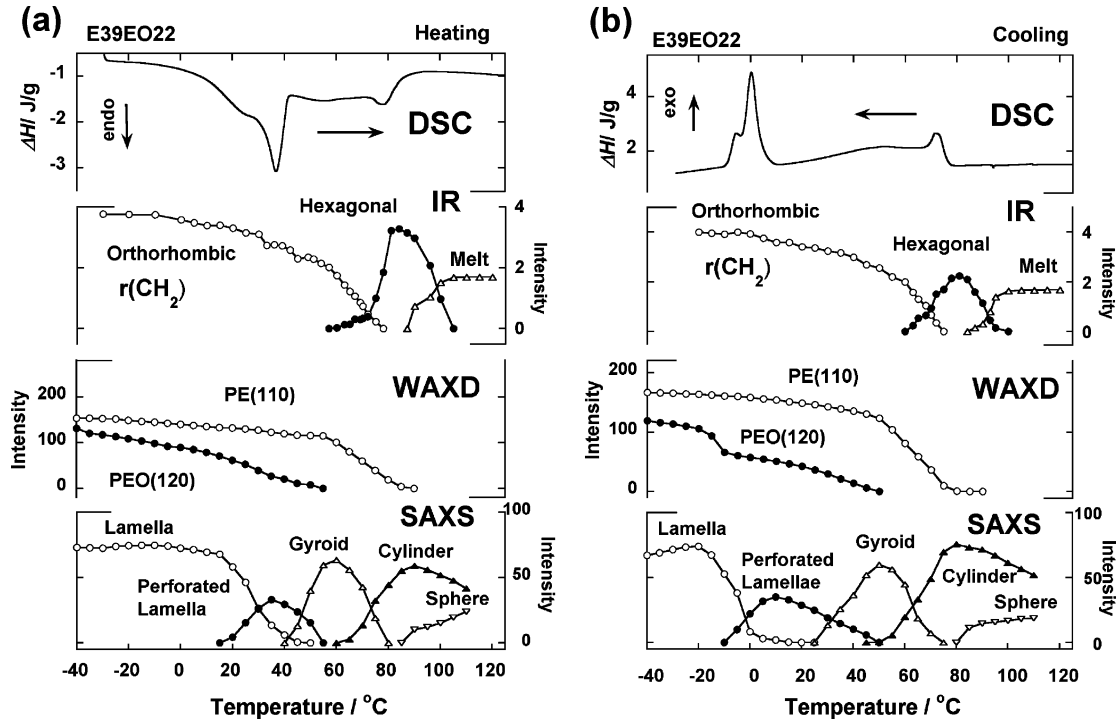

Figure 7. Temperature dependence of SAXS, WAXD, and IR intensities estimated for E39EO22 diblock copolymer in the (a) heating and (b) cooling processes.

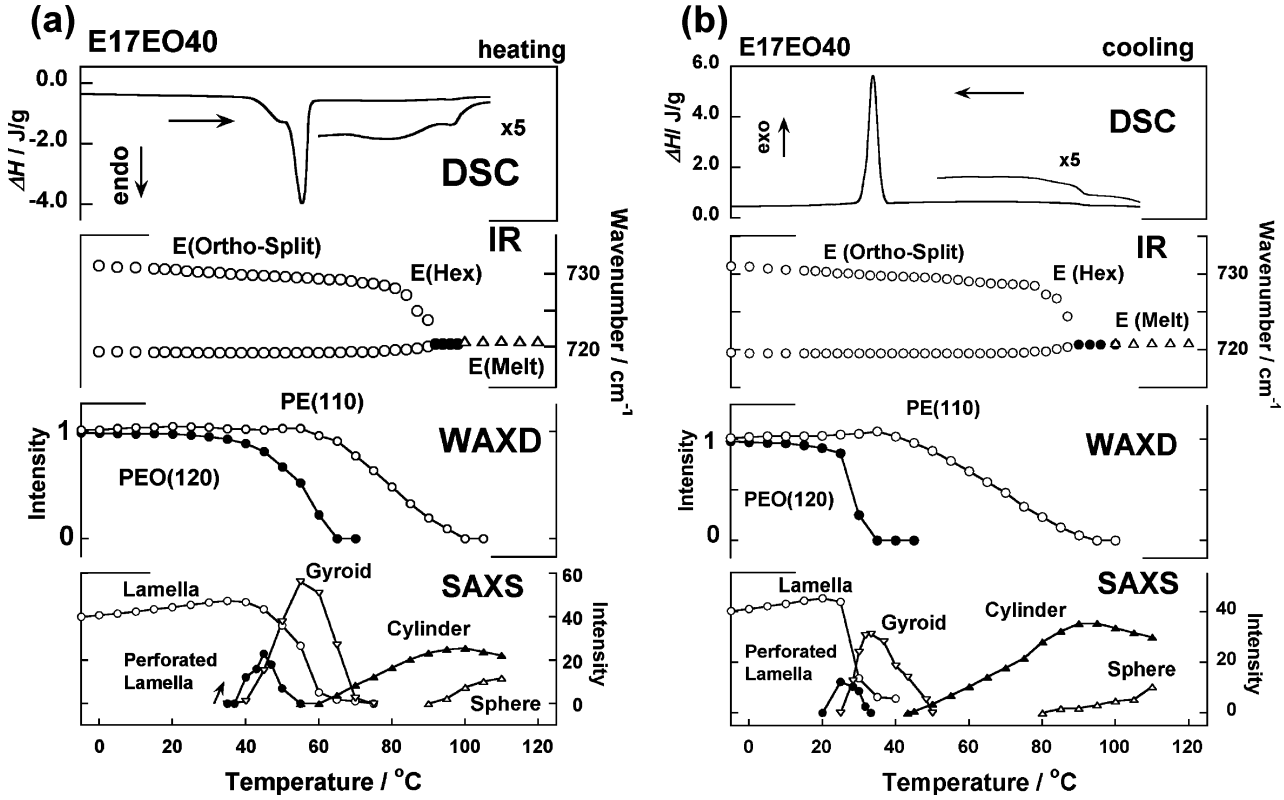

Figure 8. Temperature dependence of SAXS, WAXD, and IR intensities estimated for E17EO40 diblock copolymer in the (a) heating and (b) cooling processes.

Figure 12 shows the temperature dependence of the WAXD profile measured in the heating process. The reflections are indexed as shown there.[9] In the temperature region below 20 °C, the PE parts exist mainly as the orthorhombic phase. A broad and small peak at about 13.8 nm^{-1} is the reflection of the PEO monoclinic form, indicating that the PEO parts are hard to crystallize in this copolymer because of the spatial constraints, since the PEO segments are sandwiched between the crystalline lamellae of PE segments. A small and sharp peak was observed at about 14 nm^{-1}, which disappeared at around 50 °C. One possibility is the reflection of triclinic form of PE parts.[13] When the PEO crystallized, some stresses might be given to the already-crystallized PE orthorhombic crystal and the partial transformation to the unstable triclinic form might be induced.

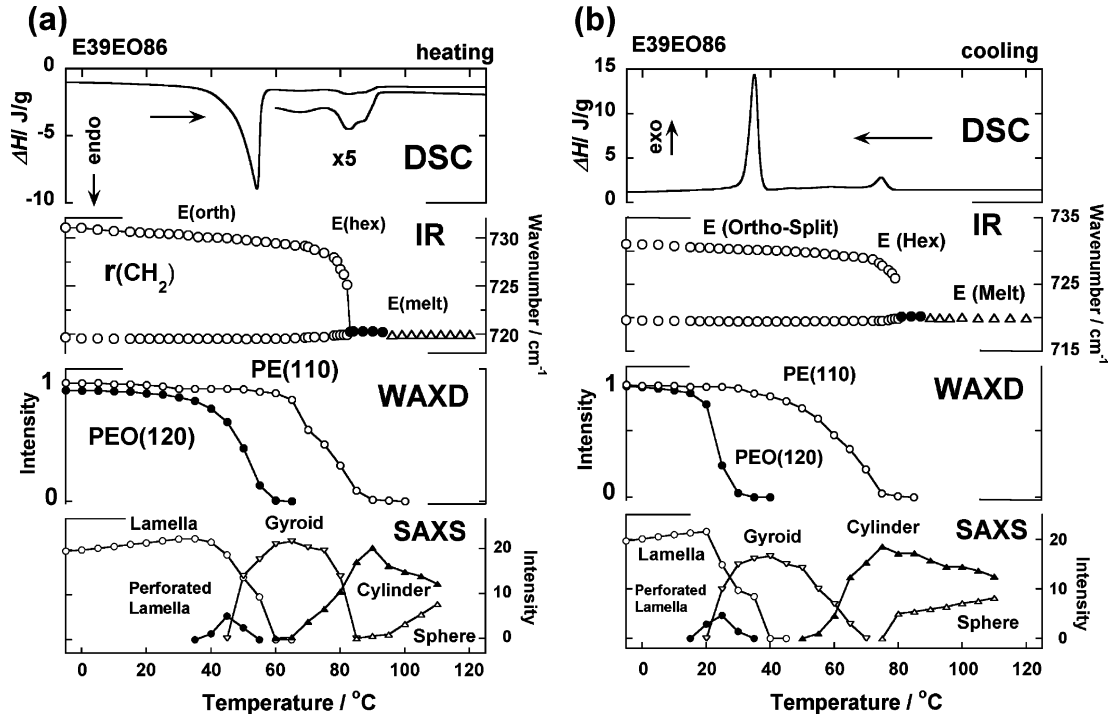

Figure 9. Temperature dependence of SAXS, WAXD, and IR intensities estimated for E39EO86 diblock copolymer in the (a) heating and (b) cooling processes.

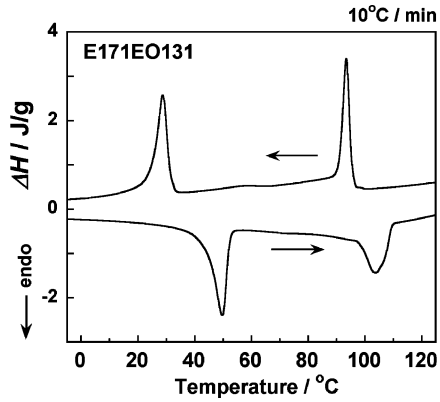

Figure 10. DSC thermograms measured for E171EO131 diblock copolymer.

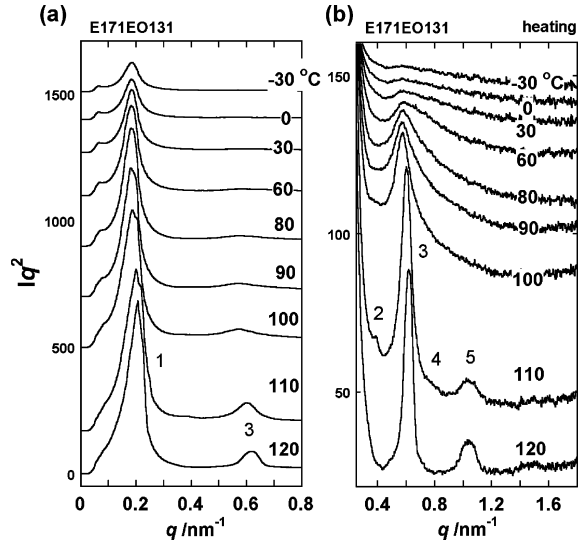

Figure 11. Temperature dependence of SAXS profiles measured for E171EO131 diblock copolymer in the heating process in the q ranges of (a) 0−0.8 nm^{-1} and (b) 0.2−1.7 nm^{-1}.

The peak disappeared when the PEO crystals were melted above 50 °C and the stresses were relaxed. The 110 reflection of PE orthorhombic phase disappeared at around 115 °C. The transition to the rotator phase could not be detected clearly because of the overlap of broad and strong amorphous halo.

Figure 13 shows the temperature dependence of infrared spectra taken in the heating process. The infrared bands of PE crystal were observed to behave in a similar way as mentioned above for the other copolymer members. As seen in Figure 13b, a pair of bands at 731 and 720 cm^{-1} are due to the correlation splitting of CH_2 rocking mode in the orthorhombic crystal of PE.[11] The 731 cm^{-1} band became weaker with increasing temperature, and the splitting width also decreased in parallel. The spectral pattern changed to that of the rotator phase immediately below the melting point, and it changed to the molten profile at higher temperature. The infrared bands of PEO segments observed at room temperature were sharper than those detected for the molten state above 50 °C. But the whole profile was different from that of the regular crystal structure (refer to Figure 6). In other words, in the temperature region between 20 °C and the melting point (∼50 °C), the PEO chains are in the conformationally disordered state. This is consistent with the WAXD data shown in Figure 12.

Figure 14 shows the temperature dependences of the various experimental data collected for E171EO131 copolymer in the heating and cooling processes. This sample takes the morphology of lamellar structure in a wide temperature region. In the narrow region of 120−85 °C the SAXS peaks are sharp and the domain of stacked lamellae is considered to spread in a wide region. In each lamella the pseudohexagonal or rotator phase is realized as known from the infrared spectral profile. As the temperature decreases below 85 °C the SAXS peaks become broader, corresponding to the smaller size of X-ray-coherent domains due to the disorder in lamellar stacking structure. The orthorhombic packing structure of PE is developed in the lamellae. The PEO lamellae are also formed at around 50 °C,

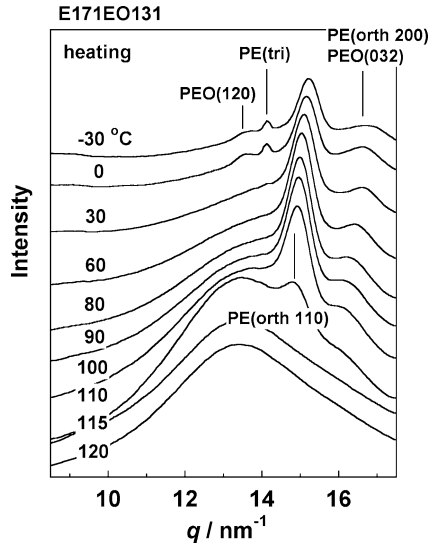

Figure 12. Temperature dependence of WAXD profiles measured for E171EO131 diblock copolymer in the heating processes.

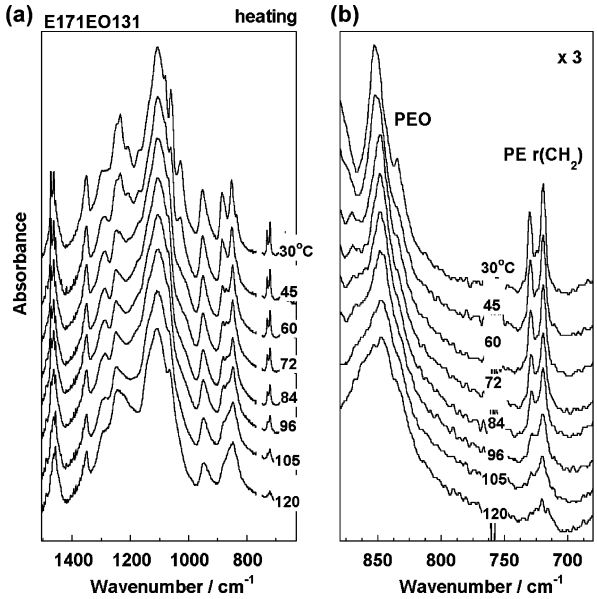

Figure 13. Temperature dependence of infrared spectra measured for E171EO131 diblock copolymer in the heating process: (a) 1500−640 cm^{-1} and (b) 870−680 cm^{-1}.

in which the conformationally disordered PEO chains are packed together. The structure became more regular, though slightly, by cooling below the room temperature. The long period of lamellae changes from 285 Å at 110 °C to 347 Å at −30 °C. In this way the E171EO131 diblock copolymer shows the disorder−order phase transitions in the PEO and PE segmental parts in the different temperature regions while maintaining the lamellar morphology. It is quite different from the above-mentioned other kinds of PE-*b*-PEO copolymers with shorter chain segments.

(4) Lamellar Structure at Low Temperature. In this way the PE-*b*-PEO diblock copolymers with relatively short and long PE chain segments show appreciably different microphase separation phenomena. The group of E17EO40, E39EO22, and E39EO86 copolymers shows the complicated transitions between lamella, perforated lamella, gyroid, cylinder, and sphere phases, while E171EO131 copolymer shows the order−disorder transitions in the lamellar morphology. Since the PEO parts are in the molten state in a high temperature region, the important factors governing these transition features are considered to come from the PE side. As a possibility, we consider the two factors, the difference in thermal mobility of PE segmental parts in higher temperature region and the inner structure of PE segments in the lamellar morphology at low temperature.

(i) Thermal Mobility. In a separate paper we measured the Raman band profiles of a diblock copolymer as a function of temperature, since the Raman bandwidth of CH_2 antisymmetric stretching mode [$\nu_{as}(CH_2)$] is sensitive to the thermal motion of PE chain.[2,5] For example, let us see the case of E39dEO25 as described in ref 2. This is the diblock copolymer consisting of PE segment of $CH_3(CH_2CH_2)_{39}-$ and deuterated PEO segment of $-(CD_2CD_2O)_{25}H$. An introduction of heavy hydrogen atoms in PEO parts was to separate the CH_2 bands of PE in the frequency region of 2900 cm^{-1} from the CD_2 bands of the PEO part in the 2200 cm^{-1} region. As shown in Figure 15, the Raman bandwidth of $\nu_{as}(CH_2)$ mode increased largely in the temperature regions where the lamella-to-gyroid and gyroid-to-cylinder transitions occurred. The larger bandwidth corresponds to the more active thermal motion of the PE chains.[5] Therefore, it may be considered reasonable that the enhancement of thermal motion of PE segments (not only the librational motion around the chain axis but also the translational motion along the interfacial boundary) is related to an induction of the morphological changes. In the case of E171EO131 copolymer, the half-width of the $\nu_{as}(CH_2)$ band of PE segment was not increased very much in a wide temperature region up to the transition point to the rotator phase. (The Raman experiment was given up at a higher temperature because of the strong fluorescence covering the weak Raman bands.) This behavior corresponds to such an observation that only the order−disorder transition occurs in PE parts by keeping the lamellar morphology. (In the case of E171EO131, the Raman data were collected without any replacement of CH_2 to CD_2 units in the PEO segments. Above room temperature the PEO segments crystallize only partially and the chain conformation is disordered, as already explained by the WAXD data. Therefore, the Raman spectral profile in the 2900 cm^{-1} region is reasonably assumed to be almost governed by only the contribution of vibrational modes of PE crystalline parts. The amorphous components of PE and PEO are included as a broad background.)

(ii) Inner Structure of Lamella. It is reasonable to consider that the inner structure of lamella is different between the PE-*b*-PEO diblock copolymers with short and long segments, which might reflect on the difference in the above-mentioned phase transition behavior as the second factor.

The long period of the stacked lamellar structure was evaluated from the SAXS peak positions measured at low temperature. For example, E39EO22 copolymer shows the first SAXS peak at 0.42 nm^{-1}, giving a long period of 149.5 Å. The chain length of E39 segment or $C_{78}H_{156}$ is calculated as 99.1 Å by assuming the planar zigzag chain conformation as supported by the infrared spectra (the effective pitch per CH_2 unit is 1.27 Å).[9] By reference to the crystal structure of *n*-alkane in which the zigzag chain is tilted by ∼35° from the normal to the lamellar surface,[14,15] the PE segment is assumed to have the thickness of about 99.1 cos(35°) = 81.2 Å. The PEO part is considered to take the (7/2) helical conformation of 19.48 Å identity period.[9] Therefore, the effective length of PEO segment is (19.48/7 monomers) × 22 monomers = 61.2 Å. The total lamellar thickness is 142.4 Å (=81.2 Å (PE) + 61.2 Å (PEO)). By considering the van der Waals radii of chain end parts of CH_3 (2.9 Å) and OH units (2.7 Å), the total thickness is 148.0 Å, which is almost the same as the observed long period 149.5

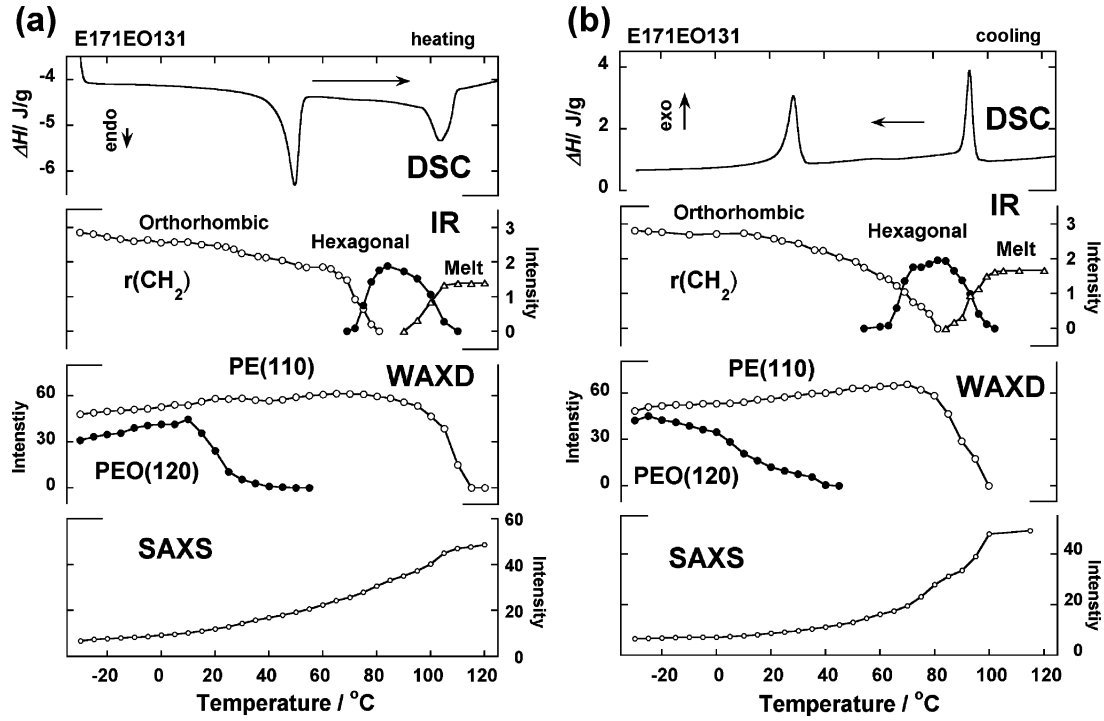

Figure 14. Temperature dependence of SAXS, WAXD, and IR intensities estimated for E171EO131 diblock copolymer in the (a) heating and (b) cooling processes.

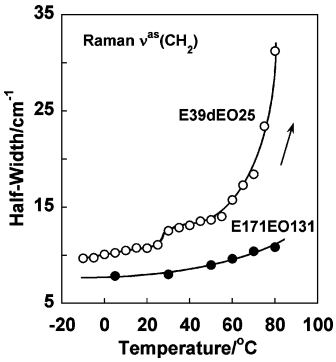

Figure 15. Temperature dependence of the half-width of $\nu_{as}(CH_2)$ Raman band measured for E171EO131 and E39dEO25 samples, where E39dEO25 contains the deuterated ethylene oxide monomers.

Å. Similarly, in the cases of E17EO40 and E39EO86, the tilted PE segmental length of planar zigzag conformation is 35.4 and 81.2 Å, and the helical length of PEO parts is 111.3 and 239.3 Å, respectively. Therefore, the total thickness including the end groups is calculated to be 152.3 and 326.1 Å, respectively. The calculated thickness 152.3 Å of E17EO40 copolymer corresponds well to the observed long period 161.0 Å. (If the tilt of the zigzag chain is ignored, the lamellar thickness is calculated to be 160.1 Å, almost the same as the observed value. But to make the discussion easier, we assume here the tilting of PE segments.) The thickness of E39EO86 copolymer is calculated to be 326.1 Å, which is overwhelmingly longer than the observed value 190.3 Å. By assuming the once-folded structure of PEO helical part, the total thickness is calculated to be 200.9 Å (=81.2 Å (PE) + 239.3/2 Å (PEO)). This calculation is rather rough because of the ignoring of the details of the folded part, but it is in relatively good agreement in order with the observed value. Figure 16 illustrates the models of lamellar structures obtained for these three kinds of PE-*b*-PEO copolymers.

A similar consideration is made for the E171EO131 copolymer. The tilted PE zigzag chain length is 355.5 Å. The regular (7/2) helical form of PEO segment gives the length 364.6 Å. The observed long period of stacked lamellar structure is 347.0 Å. By assuming the once-folded structure for both of PE and PEO parts, we should have the calculated value (355.5 + 364.6)/2 = 360.1 Å. Since the PEO parts are conformationally disordered, as pointed out in the previous section, and the stem lengths are shorter because of the chain folding, the actual PEO segment should be shorter than the simple calculation. Therefore, the once-folded model proposed for E171EO131 copolymer may be acceptable in the first approximation as illustrated in Figure 16. The effective cross-sectional areas of PE and PEO segments are not very different from each other as calculated from the crystal: about 18.2 and 21.4 Å, respectively, by referring to the unit cell sizes ($ab/2 = 7.388 \times 4.929/2 = 18.2$ Å^2 for PE and $ab \sin(\beta)/4 = (8.05)(13.04) \sin(125.4°)/4 = 21.4$ Å^2 for PEO).[9] The packing modes shown in Figure 16 are drawn by taking into consideration these situations also.

(5) Phase Transition and Lamellar Structure. As discussed above, the lamellar structure is different between the PE-*b*-PEO copolymers with short and long segments. Once the PEO segmental parts are melted at around 50 °C, the PE parts play an important role in the transition behavior of morphology. The group of PE-*b*-PEO copolymers with short PE segments shows the lamella-to-gyroid transition. The E171EO131 copolymer takes the folded structure of PE segments and shows only the order−disorder transition in a high temperature region. We may speculate here that the existence of once-folded chain structure makes the morphological transition difficult by restraining the drastic librational and translational motion of PE segments. In the case of copolymer with short PE segments, the thermal motions may occur relatively easily and the chains can move in the lateral direction along the interfacial boundary, resulting in a geometrical change of the interfacial boundary. The folded structure is speculated to make it difficult to modify the boundary shape. In many cases of crystalline−crystalline diblock copolymers, the molecular weights of polymer components are high.[4] They show only the lamellar structure up to the melting

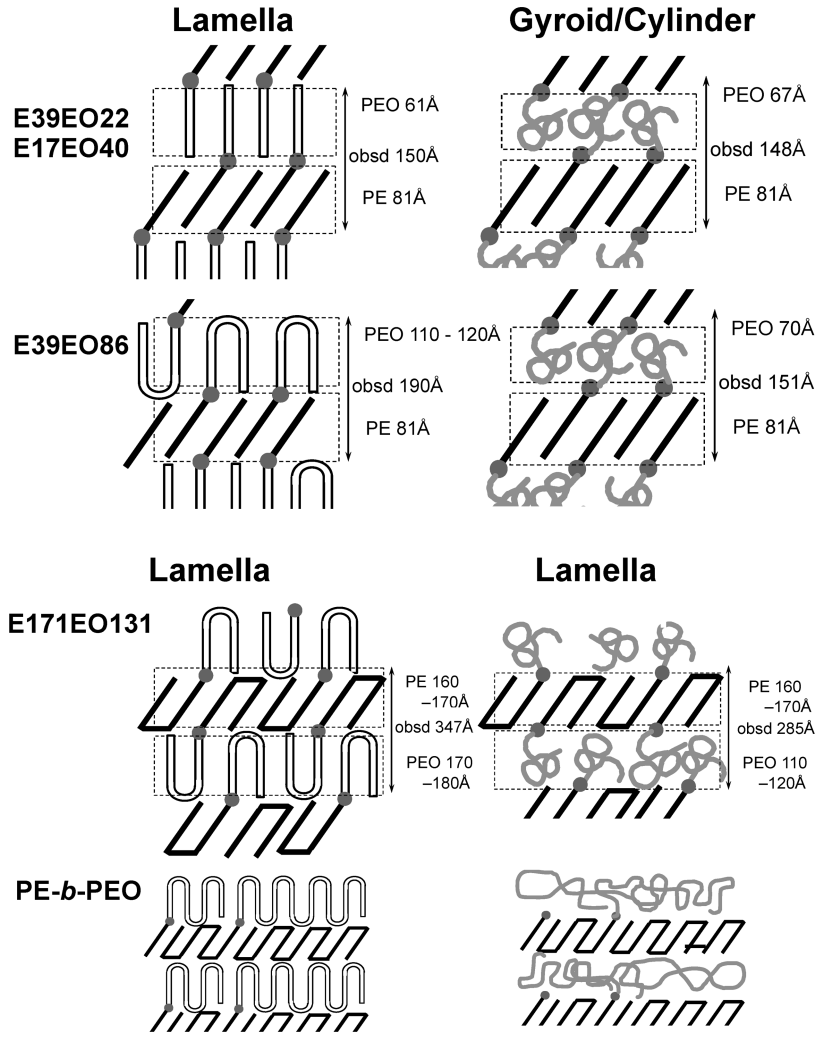

Figure 16. Schematic illustration of lamellar models for a series of PE-*b*-PEO diblock copolymer: (a) at a low temperature and (b) at a temperature above the melting point of PEO.

point. The molecular chains in the lamellae are speculated to be folded many times on the lamellar surfaces as illustrated in Figure 16. The aggregation of these folded chains may keep the surface structure flat.

The above-mentioned geometrical discussion may be a simple speculation, but it might be possible to propose here such a concept that the lamella-to-gyroid morphological change is induced by the thermally activated motion of PE segments, which is controlled by such a geometrical factor that the PE segments possess a stretched and flexible form with free end groups or they form the folded chain structure with some constraint against easy movement.

Conclusions

In the present paper we have investigated the phase transition behaviors of a series of PE-*b*-PEO diblock copolymers with the various segmental lengths. The clear difference has been detected between the groups with relatively short and rather long segmental lengths. These differences are considered to originate from the difference in the thermal mobility of the PE chains, which is related to the chain form taken in the starting lamellae at a low temperature. The short copolymer exhibits the packing structure consisting of straight segments with free ends. These chains can move to some extent in the lamella because of the enhancement of thermal motion: a librational motion around the chain axis and a translational motion along the interfacial surface. On the other hand, the long copolymer shows the packing structure of stems with the folded parts on the lamellar surfaces. Such a geometrical constraint is speculated to suppress the thermal motion and make it difficult to induce the transition from lamellar to gyroid morphology. This concept may explain also the characteristic feature of general crystalline−crystalline (and crystalline−amorphous) diblock copolymers with chain components of high molecular weights: the lamella-to-gyroid transition is difficult to occur as long as the chain-folded lamellar structure exists, as observed in the actual experiments.[3,4] The molecular dynamics simulation, for example, might help us to confirm this concept of a trigger for the phase transition phenomenon of diblock copolymers.

The theoretical treatment of microphase separation had been made so far by assuming the continuous bodies for the two segmental parts with the random coil conformations. The theory takes into consideration the interactions between these two continuous bodies using a Flory−Huggins χ parameter.[16] But the present study requests us to consider the packing structure of polymer segments in the crystalline lamellae for the interpretation of the observed transition phenomena, where the morphological changes are dependent on the chain length of the segments, which affects the inner structure and the chain folding on the surface. At present, however, the authors do not

have any idea how to introduce these concrete geometrical constraints into the theory of microphase separation phenomenon.

Acknowledgment. This research was financially supported by a MEXT "Collaboration with Local Communities" Project (2005−2009).

References and Notes

(1) Cao, W. Y.; Tashiro, K.; Hanesaka, M.; Takeda, S.; Masunaga, H.; Sasaki, S.; Takata, M. *J. Phys. Chem. B* **2009**, *113*, 2338.

(2) Cao, W. Y.; Tashiro, K.; Hanesaka, M.; Takeda, S.; Masunaga, H.; Sasaki, S.; Takata, M. *Polym. Prepr. Jpn.*, in press.

(3) (a) Rangarajan, P.; Register, R. A.; Fetters, L. J. *Macromolecules* **1993**, *26*, 4640. (b) Rangarajan, P.; Register, R. A.; Adamson, D. H.; Fetters, L. J.; Bras, W.; Naylor, S.; Ryan, A. J. *Macromolecules* **1995**, *28*, 1422. (c) Rangarajan, P.; Register, R. A.; Fetters, L. J.; Bras, W.; Naylor, S.; Ryan, A. J. *Macromolecules* **1995**, *28*, 4932. (d) Richter, D.; Schneiders, D.; Monkenbusch, M.; Willner, L.; Fetters, L. J.; Huang, J. S.; Lin, M.; Mortensen, K.; Farago, B. *Macromolecules* **1997**, *30*, 1053. (e) Hamley, I. W. *Adv. Polym. Sci.* **1999**, *148*, 113. (f) Hamley, I. W.; Fairclough, J. P. A.; Ryan, A. J.; Mai, S. M.; Booth, C. *Phys. Chem. Chem. Phys.* **1999**, *1*, 2097. (g) Zhu, L.; Calhoun, B. H.; Ge, Q.; Quirk, R. P.; Cheng, Z.; Thomas, E. L.; Hsiao, B. S.; Yeh, F.; Liu, L.; Lotz, B. *Macromolecules* **2001**, *34*, 1244. (h) Zhu, L.; Cheng, S. Z. D.; Calhoun, B. H.; Ge, Q.; Quirk, R. P.; Thomas, E. L.; Hsiao, B. S.; Yeh, F; Lotz, B. *Polymer* **2001**, *42*, 5829. (i) Loo, Y. L.; Register, R. A.; Ryan, A. J *Macromolecules* **2002**, *35*, 2365. (j) Hamley, I. W.; Castelletto, V.; Floudas, G.; Schipper, F. *Macromolecules* **2002**, *35*, 8839.

(4) (a) Shiomi, T.; Imai, K.; Takenaka, K.; Takeshita, H.; Hayashi, H.; Tezuka, Y. *Polymer* **2001**, *42*, 3233. (b) Fujiwara, T.; Miyamoto, M.; Kimura, Y.; Iwata, T.; Doi, Y. *Macromolecules* **2001**, *34*, 4043. (c) Ho, R.-M.; Hsieh, P.-Y.; Tseng, W.-H.; Lin, C.-C.; Huang, B.-H.; Lotz, B. *Macromolecules* **2003**, *36*, 9085. (d) Nojima, S.; Akutsu, Y.; Akaba, M.; Tanimoto, S. *Polymer* **2005**, *46*, 4060. (e) Takeshita, H.; Fukumoto, K.; Ohnishi, T.; Ohkubo, T.; Miya, M.; Takenaka, K.; Shiomi, T. *Polymer* **2006**, *47*, 8210. (f) Nojima, S.; Kiji, T.; Ohguma, Y. *Macromolecules* **2007**, *48*, 7566. (g) Nojima, S.; Ito, K.; Ikeda, H. *Polymer* **2007**, *48*, 3607. (h) Müller, A. J.; Balsamo, V.; Arnal, M. L. *Adv. Polym. Sci.* **2005**, *190*, 1. (i) Loo, Y. L.; Register, R. A. Crystallization within Block Copolymer Mesophases. In *Developments in Block Copolymer Science and Technology*; Hamley, I. W., Ed.; Wiley: New York, 2004; Chapter 6, pp 213−243. (j) Müller, A. J.; Balsamo, V.; Arnal, M. L. *Lect. Notes Phys.* **2007**, *714*, 229.

(5) (a) Snyder, R. G.; Scherer, J. R.; Gaber, B. P. *Biochim. Biophys. Acta* **1980**, *601*, 47. (b) MacPhail, R. A.; Snyder, R. G.; Strauss, H. *J. Chem. Phys.* **1982**, *77*, 1118. (c) Casal, H. L.; Cameron, D. G.; Kelusky, E. C.; Tulloch, A. P. *J. Chem. Phys.* **1984**, *81*, 4322. (d) Kobayashi, M.; Koizumi, H.; Cho, Y. *J. Chem. Phys.* **1990**, *93*, 4659.

(6) (a) Sun, L.; Liu, Y.; Zhu, L.; Hsiao, B. S.; Avila-Orta, C. A. *Polymer* **2004**, *45*, 8181. (b) Sun, L.; Liu, Y.; Zhu, L.; Hsiao, B. S.; Avila-Orta, C. A. *Macromol. Rapid Commun.* **2004**, *25*, 853.

(7) Castillo, R. V.; Arnal, M. L.; Muller, A. J.; Hamley, I. W.; Castelletto, V.; Schmalz, H.; Abetz, V. *Macromolecules* **2008**, *41*, 879.

(8) (a) Hamley, I. W. *The Physics of Block Copolymers*; Oxford University Press: New York, 1998. (b) Hamley, I. W.; Castelletto, C. *Prog. Polym. Sci.* **2004**, *29*, 909.

(9) (a) Tadokoro, H. *Structure of Crystalline Polymers*; Wiley: New York, 1979. (b) Tadokoro, H.; Chatani, Y.; Yoshihara, T.; Tahara, S.; Murahashi, S. *Macromol. Chem.* **1964**, *73*, 109. (c) Takahashi, Y.; Tadokoro, H. *Macromolecules* **1973**, *6*, 672.

(10) (a) Tashiro, K.; Sasaki, S.; Kobayashi, M. *Macromolecules* **1996**, *29*, 7460. (b) Snyder, R. G.; Maroncelli, M.; Qi, S. P.; Strauss, H. L. *Science* **1981**, *214*, 188. (c) Maroncelli, M.; Qi, S. P.; Strauss, H. L.; Snyder, R. G. *J. Am. Chem. Soc.* **1982**, *104*, 6327.

(11) (a) Krimm, S.; Liang, C. Y.; Sutherland, G. B. B. M. *J. Chem. Phys.* **1956**, *25*, 549. (b) Tasumi, M.; Shimanouchi, T. *J. Chem. Phys.* **1965**, *43*, 1245.

(12) Morishita, H.; Kobayashi, M.; Sato, K.; Kondo, H.; Suharto, M. *Nagasaki Daigaku Kyoikugakubu Shizen Kagaku Kenkyu Hokoku* **1995**, *52*, 13.

(13) (a) Seto, T.; Hara, T.; Tanaka, K. *Jpn. J. Appl. Phys.* **1968**, *35*, 1599. (b) Muller, A.; Lonsdale, K. *Acta Crystallogr.* **1948**, *1*, 129. (c) Hayashida, T. *J. Phys. Soc. Jpn.* **1962**, *17*, 306. (d) Nyburg, S. C.; Luth, H. *Acta Crystallogr.* **1972**, *B28*, 2992.

(14) Ungar, G.; Stejny, J.; Keller, A.; Bidd, I.; Whiting, M. C. *Science* **1985**, *229*, 4711.

(15) Ungar, G.; Zeng, X. B.; Spells, S. J. *Polymer* **2000**, *41*, 8775.

(16) (a) Helfand, E. *Macromolecules* **1975**, *8*, 522. (b) Leibler, L. *Macromolecules* **1980**, *13*, 1602. (c) Fredrickson, G. H.; Ganesan, V.; Drolet, F. *Macromolecules* **2002**, *35*, 16.

JP901442A